Multibody Syst Dyn (2008) 20: 287–306
DOI 10.1007/s11044-008-9120-8

# Analysis of dynamic strains in tibia during human locomotion based on flexible multibody approach integrated with magnetic resonance imaging technique

**R. Al Nazer · A. Klodowski · T. Rantalainen · A. Heinonen · H. Sievänen · A. Mikkola**

Received: 28 January 2008 / Accepted: 18 June 2008 / Published online: 23 July 2008


**Abstract** Bone is known to adapt to the prevalent strain environment while the variation in strains, e.g., due to mechanical loading, modulates bone remodeling, and modeling. Dynamic strains rather than static strains provide the primary stimulus of bone functional adaptation. The finite element method can be generally used for estimating bone strains, but it may be limited to the static analysis of bone strains since the dynamic analysis requires expensive computation. Direct in vivo strain measurement, in turn, is an invasive procedure, limited to certain superficial bone sites, and requires surgical implementation of strain gauges and thus involves risks (e.g., infection). Therefore, to overcome difficulties associated with the finite element method and the in vivo strain measurements, the flexible multibody simulation approach has been recently introduced as a feasible method to estimate dynamic bone strains during physical activity. The purpose of the present study is to further strengthen the idea of using the flexible multibody approach for the analysis of dynamic bone strains. Besides discussing the background theory, magnetic resonance imaging is integrated into the flexible multibody approach framework so that the actual bone geometry could be better accounted for and the accuracy of prediction improved.

**Keywords** Bone · Flexible multibody dynamics · Tibia · Locomotion · Strain estimation · MRI

R. Al Nazer (✉) · A. Klodowski · T. Rantalainen · A. Mikkola
Department of Mechanical Engineering, Lappeenranta University of Technology, Lappeenranta, Finland
e-mail: alanazer@lut.fi

T. Rantalainen
Neuromuscular Research Center, Department of Biology of Physical Activity, University of Jyväskylä, Jyväskylä, Finland

A. Heinonen
Department of Health Sciences, University of Jyväskylä, Jyväskylä, Finland

H. Sievänen
Bone Research Group, UKK Institute, Tampere, Finland

## 1 Introduction

A skeleton's capacity to withstand external loading is achieved and maintained through adaptive remodeling of bone tissue [1]. Based on previous studies, the bone adaptive process relies on dynamic bone strains rather than static strains [2, 3]. In order to quantify the mechanical loading environment of the skeleton, the in vivo implementation of strain gauges on bone surfaces, such as the anterior surface of the tibia or radius, have been used previously [4–6]. However, measuring bone strains in vivo is invasive, which is challenging and not feasible for the majority of bones.

Computer models and simulation of the musculoskeletal system provide a realistic and economical approach to add a valuable dimension to biomechanical, medical research, and training. Numerous models have been used to predict or estimate characteristics of human mechanisms in body movement and simulate surgical treatments. Experimental data can be used as a source of model input parameters and for evaluating the validity of a given model. Biomechanical models based on multibody dynamics have been used widely in the analysis of human physical activities [7] and the biomechanical consequences of surgical reconstructions such as joint replacements [8] and tendon transfer [9]. Spagele et al. [10] have developed a human lower limb model consisting of three rigid bodies and nine musculotendon actuators to simulate a human jump. A three-dimensional human skeletal model consisting of 16 rigid bodies with 35 degrees of freedom has been developed by Nagano et al. [11] to simulate motion during the flight phase of a horizontal jump. In addition, multibody biomechanical models have been applied to passive human motion in order to study different injury scenarios such as impact or falling down. For example, Silva et al. [12] have studied injury scenarios for the human head during impact simulation in different vehicle crash situations and the offside tackle of an athlete using a three-dimensional biomechanical model consisting of 12 rigid bodies coupled by 11 kinematic joints with passive torque applied at each joint. The same biomechanical model described previously by Silva et al. [12] is used in the work of Ambrósio and Silva [13] to investigate the whiplash injury scenario for three occupants during a roll over of an all-terrain vehicle simulation. Biomechanical multibody models of humans are typically more complicated than other multibody systems, as they involve a larger variety of joint types, body or bone forms, and complex actuators formed by muscles and related soft tissues. Therefore, commercial softwares specialized in building human musculoskeletal models, such as SIMM [9], have been used to enhance the development of biomechanical modeling. In all of the above-mentioned studies, bones are assumed to be rigid bodies, a fact that renders these models unfeasible for bone strain analysis.

Bone strains have been generally analyzed using the finite element method. For example, Duda et al. [14] constructed a femoral finite element model obtained from successive Computed Tomography (CT) scans to study the influence of muscle forces on femoral strain distribution during gait. In the work of Cheung et al. [15], a three-dimensional finite element model of the foot and ankle is developed based on Magnetic Resonance Imaging (MRI) data to investigate the internal stresses/strains within bones and soft tissues of the ankle and foot under various loadings. However, due to the complex bone geometry, finite element models used in the stress analysis require fine element meshes that will result in a large number of nodal degrees of freedom. For this reason, the numerical solutions of these models are computationally expensive, limiting the finite element analyses only to a bone segment or a single bone. It is also noteworthy that, due to the expensive computation, finite element models are usually applied to a static or short term dynamic solution. Accordingly, the finite element method is computationally impractical for dynamic analysis of human

musculoskeletal models where the number of bones and muscles as well as their interaction needs to be taken into consideration.

The objective of this study is to extend the idea of using the flexible multibody simulation approach for dynamic analysis of bone strains by integrating the magnetic resonance (MR) imaging data into the framework. In their study, Al Nazer et al. [16] showed that the flexible multibody simulation approach can be reasonably used to predict dynamic bone strains during physical activity. In the study, a lower-body musculoskeletal model with a flexible tibia was used as a demonstration to predict the tibial strains during level walking. However, the flexible tibial model was based on a generic model of anthropometric variables accessible through the commercial software [17]. Further, the previous finite element model of the tibia was meshed using a shell element with a thickness equal to the average cortical wall thickness of the subject's tibial mid-shaft. In this study, the lower body musculoskeletal model introduced by Al Nazer et al. [16] is used as a demonstration to simulate level walking in order to predict the tibial strains. However, the flexible bone model is based on the actual geometry of the subject's tibia, which is obtained from a three-dimensional reconstruction of MRI data.

## 2 Modeling of flexible skeleton

The methods available in the literature to study mechanical flexibility in a multibody system can be categorized into four approaches. In the first approach, the nonlinear finite element formulations such as the absolute nodal coordinate formulation [18] and large rotational vector formulation [19] are embedded in the multibody formalism in order to describe mechanical flexibility. In the second approach, the linear theory of elastodynamics [18] where the deformations and rigid body motion are uncoupled is used in the description of mechanical flexibility. The third is the lumped mass approach [18] in which a set of rigid bodies with intervenient force elements are used to describe flexibility of mechanical components. Finally, the fourth approach applies the floating frame of reference formulation [18] which is based on the concept of the reference coordinate system. The use of the reference frame allows to couple deformations and large reference motions of the flexible body. Usually, the deformations in the floating frame of reference formulation are assumed to be linear with respect to the reference frame. The assumption makes it possible to use modal coordinates instead of nodal coordinates in the description of flexible body deformations. The number of modal coordinates is often much lower than the number of nodal coordinates. For this reason, the use of modal coordinates decreases the computational cost with a minimum loss of accuracy [18]. Therefore, for a multibody system in which the geometries of the bodies are complicated and small deformations are expected with large translation and rotations, the floating frame of reference formulation may be the best choice [19]. It is worth mentioning that the strains of the bone can also be calculated using the linear theory of elastodynamics [18]. In this approach, the bone is assumed to be a rigid body in the multibody simulation. The results of the multibody simulation (that are muscle, ground reaction and inertia forces of the bone) are used in the detailed finite element model of the bone to calculate strains after the dynamic analysis. However, in this approach, the deformation and large rigid body motion are not coupled, leading to an unnatural solution. In addition, it would be difficult to define boundary conditions in the finite element model so that they accurately represent constraints used in the multibody simulation.

Human bones have complex shapes, and during a variety of movements, bones experience large translational and rotational displacements while deformations within bones remain small—of the order of 3,000 microstrain at maximum [5]. As a result, the multibody

simulation approach with the floating frame of reference formulation is the most appropriate approach to estimate tibial deformations during exercise. In the floating frame of reference approach, the configuration of the flexible tibia is identified by using two sets of coordinates; reference and nodal coordinates, which can be described as follows:

$$\mathbf{q}^i = \begin{bmatrix} \mathbf{q}_{\mathrm{r}}^i & \mathbf{q}_{\mathrm{f}}^i \end{bmatrix}^{\mathrm{T}} \tag{2.1}$$

where $\mathbf{q}^i$ is the vector of generalized coordinates of the flexible tibia, $\mathbf{q}_{\mathrm{r}}^i$ is the vector of reference coordinates which defines the large translation and rotation of the flexible tibia with respect to the global coordinate system, and $\mathbf{q}_{\mathrm{f}}^i$ is the vector of nodal coordinates which defines the deformation of the tibia with respect to the flexible tibia coordinate system. Hereafter, the subscript $i$ corresponds to the flexible tibia. In this study, only the components of the equations of motion of the flexible tibia are shown.

## 2.1 Component mode synthesis

Due to the complex geometry of the tibia, the tibial finite element model consists of a large number of nodal degrees of freedom, which makes it computationally expensive to define the deformations in the time domain analyses. This computational problem can be alleviated using the component mode synthesis [20]. As a result, the deformation of the tibia can be described using deformation shape modes instead of nodal coordinates. The dimensionality of the tibial finite element model (i.e., degrees of freedom) can be reduced by solving for $m$ deformation modes only, where $m \ll n$ (nodal coordinates). A reduced order model of the flexible tibia can be described using $m$ deformation modes as follows [18]:

$$\mathbf{q}_{\mathrm{f}}^i = \boldsymbol{\Phi}^i \mathbf{p}^i \tag{2.2}$$

where $\boldsymbol{\Phi}^i$ is the modal transformation matrix whose columns are the selected $m$ tibial deformation modes and $\mathbf{p}^i$ is the modal coordinates associated with the deformation modes. In this study, the deformation modes defined in (2.2) are calculated by employing the Craig–Bampton method with the orthonormalization procedure [21], which yields the orthogonal Craig–Bampton modes. The Craig–Bampton method represents one of the component mode synthesis techniques, which has been employed in a number of applications. This method applies a simple and straightforward procedure to obtain deformation modes capable of giving highly accurate dynamic solutions with efficient computational time as compared to the other methods such as the attachment mode method [20]. Therefore, the Craig–Bampton method has been used in a number of multibody simulation codes. In the Craig–Bampton method, the vector of nodal coordinates of the tibial finite element model is partitioned into boundary and interior nodal coordinates. The equation of motion of the tibial finite element model can be defined as follows:

$$\mathbf{m}_{\mathrm{f}}^i \ddot{\mathbf{q}}_{\mathrm{f}}^i + \mathbf{K}_{\mathrm{f}}^i \mathbf{q}_{\mathrm{f}}^i = \mathbf{F}_{\mathrm{f}}^i \tag{2.3}$$

where $\mathbf{m}_{\mathrm{f}}^i$ and $\mathbf{K}_{\mathrm{f}}^i$ are the finite element mass and stiffness matrices of the flexible tibia respectively and $\mathbf{F}_{\mathrm{f}}^i$ is the vector of external force associated with the nodal coordinates of the flexible tibia. Based on the Craig–Bampton partitioning, (2.3) can be expressed in the following form:

$$\begin{bmatrix} \mathbf{m}_{\mathrm{BB}}^i & \mathbf{m}_{\mathrm{BI}}^i \\ \mathbf{m}_{\mathrm{IB}}^i & \mathbf{m}_{\mathrm{II}}^i \end{bmatrix} \begin{bmatrix} \ddot{\mathbf{q}}_{\mathrm{fB}}^i \\ \ddot{\mathbf{q}}_{\mathrm{fI}}^i \end{bmatrix} + \begin{bmatrix} \mathbf{K}_{\mathrm{BB}}^i & \mathbf{K}_{\mathrm{BI}}^i \\ \mathbf{K}_{\mathrm{IB}}^i & \mathbf{K}_{\mathrm{II}}^i \end{bmatrix} \begin{bmatrix} \mathbf{q}_{\mathrm{fB}}^i \\ \mathbf{q}_{\mathrm{fI}}^i \end{bmatrix} = \begin{bmatrix} \mathbf{F}_{\mathrm{fB}}^i \\ \mathbf{F}_{\mathrm{fI}}^i \end{bmatrix} \tag{2.4}$$

where the subscripts B and I correspond to the boundary and interior nodal coordinates, respectively. The Craig–Bampton method results in two sets of modes, which are nonorthogonal constraint modes and orthogonal fixed interface normal modes. The constraint modes describe deformation due to unit displacements of boundary nodal coordinates and they can be obtained from a static equilibrium analysis of the tibial finite element model equation of motion expressed in (2.4). As a result of applying a static equilibrium analysis, (2.4) can be rewritten as follows:

$$\begin{bmatrix} \mathbf{F}^i_{\mathrm{fB}} \\ \mathbf{F}^i_{\mathrm{fI}} \end{bmatrix} = \begin{bmatrix} \mathbf{K}^i_{\mathrm{BB}} & \mathbf{K}^i_{\mathrm{BI}} \\ \mathbf{K}^i_{\mathrm{IB}} & \mathbf{K}^i_{\mathrm{II}} \end{bmatrix} \begin{bmatrix} \mathbf{q}^i_{\mathrm{fB}} \\ \mathbf{q}^i_{\mathrm{fI}} \end{bmatrix} \tag{2.5}$$

The constraint modes can be extracted from the previous equation assuming that the interior forces are set to zero as follows:

$$\begin{bmatrix} \mathbf{F}^i_{\mathrm{fB}} \\ \mathbf{0} \end{bmatrix} = \begin{bmatrix} \mathbf{K}^i_{\mathrm{BB}} & \mathbf{K}^i_{\mathrm{BI}} \\ \mathbf{K}^i_{\mathrm{IB}} & \mathbf{K}^i_{\mathrm{II}} \end{bmatrix} \begin{bmatrix} \mathbf{q}^i_{\mathrm{fB}} \\ \mathbf{q}^i_{\mathrm{fI}} \end{bmatrix} \tag{2.6}$$

Consequently:

$$\mathbf{q}^i_{\mathrm{fI}} = \left[-\mathbf{K}^i_{\mathrm{II}}\right]^{-1} \mathbf{K}^i_{\mathrm{IB}} \mathbf{q}^i_{\mathrm{fB}} = \mathbf{\Phi}^i_{\mathrm{C}} \mathbf{q}^i_{\mathrm{fB}} \tag{2.7}$$

where $\mathbf{\Phi}^i_{\mathrm{C}}$ is the matrix whose columns are non-orthogonal constraint modes. The fixed interface normal modes describe vibration modes when fixed boundary conditions are applied at all the boundary nodal coordinates. The fixed interface normal modes can be obtained by solving an eigenvalue analysis of (2.4) as follows:

$$\left[-\left(\omega^{iN}\right)^2 \mathbf{m}^i_{\mathrm{II}} + \mathbf{K}^i_{\mathrm{II}}\right] \mathbf{a}^{iN} = \mathbf{0} \tag{2.8}$$

where $\omega^{iN}$ is a set of eigenvalues or natural frequencies associated with the eigenvectors $\mathbf{a}^{iN}$. Those eigenvectors are called the fixed interface normal modes. The combination of the constraint modes and fixed interface normal modes yields the nonorthogonal Craig–Bampton deformation modes. Assembling the nonorthogonal Craig–Bampton modes in a matrix yields the matrix whose columns are the non-orthogonal Craig–Bampton modes as follows:

$$\mathbf{\Phi}^i_{\mathrm{CB}} = \begin{bmatrix} \mathbf{I} & \mathbf{0} \\ \mathbf{\Phi}^i_{\mathrm{C}} & \mathbf{\Phi}^i_{\mathrm{N}} \end{bmatrix} \tag{2.9}$$

where $\mathbf{\Phi}^i_{\mathrm{N}}$ is the matrix of fixed interface normal modes. It is essential to emphasize here that the nonorthogonal Craig–Bampton modes expressed in (2.9) are not orthogonal with respect to the finite element mass and stiffness matrices. Therefore, the orthonormalization procedure is applied to the Craig–Bampton modes in order to enforce their orthogonality. The subsequent orthogonal Craig–Bampton can be assembled in a matrix in order to obtain the matrix whose columns are the orthogonal Craig–Bampton modes which can be used to transform nodal coordinates to modal coordinates, as it was previously shown in (2.2). The matrix can be defined as follows:

$$\mathbf{\Phi}^i = [\, \mathbf{b}^i_1 \quad \cdots \quad \mathbf{b}^i_m \,] \tag{2.10}$$

where $\mathbf{b}^i_m$ is the $m$th orthogonal Craig–Bampton mode. The orthogonal Craig–Bampton modes defined in the previous equation can be normalized with respect to the mass matrix

of the non-orthogonal Craig–Bampton modes expressed in (2.13), and thus the diagonal mass and stiffness matrices can be expressed in the following forms:

$$\mathbf{m}_{\mathrm{pp}}^{i} = \boldsymbol{\Phi}^{i\mathrm{T}} \mathbf{m}_{\mathrm{CB}}^{i} \boldsymbol{\Phi}^{i} = \mathbf{I} \tag{2.11}$$

$$\mathbf{K}_{\mathrm{pp}}^{i} = \boldsymbol{\Phi}^{i\mathrm{T}} \mathbf{K}_{\mathrm{CB}}^{i} \boldsymbol{\Phi}^{i} = \begin{bmatrix} \omega_1^{i*2} & & 0 \\ & \ddots & \\ 0 & & \omega_m^{i*2} \end{bmatrix} \tag{2.12}$$

where $\mathbf{m}_{\mathrm{pp}}^{i}$ and $\mathbf{K}_{\mathrm{pp}}^{i}$ are the diagonal modal mass and stiffness matrices based on the orthogonal Craig–Bampton modes, respectively, $\omega^{i*}$ is a set of eigenvalues or natural frequencies of the selected $m$ orthogonal Craig–Bampton modes of the flexible tibia and $\mathbf{m}_{\mathrm{CB}}^{i}$ and $\mathbf{K}_{\mathrm{CB}}^{i}$ are the modal mass and stiffness matrices associated with nonorthogonal Craig–Bampton modes, respectively. These matrices can, respectively, be defined as follows:

$$\mathbf{m}_{\mathrm{CB}}^{i} = \boldsymbol{\Phi}_{\mathrm{CB}}^{i\mathrm{T}} \mathbf{m}_{\mathrm{f}}^{i} \boldsymbol{\Phi}_{\mathrm{CB}}^{i} \tag{2.13}$$

$$\mathbf{K}_{\mathrm{CB}}^{i} = \boldsymbol{\Phi}_{\mathrm{CB}}^{i\mathrm{T}} \mathbf{K}_{\mathrm{f}}^{i} \boldsymbol{\Phi}_{\mathrm{CB}}^{i} \tag{2.14}$$

## 2.2 Equations of motion

The biomechanical multibody model presented in this study consists of interconnected rigid and flexible bodies. The equations of motion of such a multibody system can be expressed as follows [18]:

$$\mathbf{M}\ddot{\mathbf{q}} + \mathbf{K}\mathbf{q} + \mathbf{C}_{\mathbf{q}}^{\mathrm{T}} \boldsymbol{\lambda} = \mathbf{Q}_{\mathrm{e}} + \mathbf{Q}_{\mathrm{v}} \tag{2.15}$$

where $\mathbf{q}$ is the vector of the generalized coordinates of all bodies in the biomechanical model, $\mathbf{C}_{\mathbf{q}}$ is the Jacobian matrix of the nonlinear constraints equation and $\boldsymbol{\lambda}$ is the vector of Lagrange multipliers. In (2.15), $\mathbf{Q}_{\mathrm{v}}$ is the vector that describes the quadratic velocity inertia forces which can be defined using the expression of the virtual work of the inertial forces and $\mathbf{M}$ is the mass matrix of the biomechanical model which can be defined using kinetic energy. The generalized forces acting on the biomechanical model are divided into two types; the external forces and the elastic forces. External forces $\mathbf{Q}_{\mathrm{e}}$ in (2.15) are the forces produced by the muscles and gravity. The elastic forces $\mathbf{K}\mathbf{q}$ in (2.15) are due to the deformation of the flexible tibia. The vector of elastic forces associated with the generalized coordinates of the flexible tibia can be expressed as follows:

$$\mathbf{Q}_{\mathrm{s}}^{i} = -\mathbf{q}^{i\mathrm{T}} \mathbf{K}^{i} \tag{2.16}$$

where $\mathbf{K}^{i}$ is the generalized stiffness matrix of the flexible tibia which can be defined as follows:

$$\mathbf{K}^{i} = \begin{bmatrix} 0 & 0 & 0 \\ \vdots & \ddots & \vdots \\ 0 & \cdots & \mathbf{K}_{\mathrm{pp}}^{i} \end{bmatrix} \tag{2.17}$$

Equation (2.15) represents a system of second-order differential equations whose solution must satisfy the algebraic constraint equations during the dynamic simulation. The algebraic constraint equations which describe the mechanical joints of the bodies in the model as well as their specified trajectories can be expressed as follows:

$$\mathbf{C}(\mathbf{q}, t) = \mathbf{0} \tag{2.18}$$

where $t$ is the time and $\mathbf{C}$ is the vector of linearly independent nonlinear constraint equations of the biomechanical model. Equations (2.15) and (2.18) represent a set of nonlinear differential algebraic equations DAE which have to be solved simultaneously. Having solved for the modal coordinates from (2.15), the strain vector of the flexible body, $\boldsymbol{\varepsilon}^i$, can be obtained as a post-processing procedure as follows:

$$\boldsymbol{\varepsilon}^i = \mathbf{D}^i \boldsymbol{\Phi}^i \mathbf{p}^i$$

where $\mathbf{D}^i$ is the kinematics matrix that describes the strain-displacement relationship. The matrix can be obtained using the shape function matrix. The strain-displacement relationship described by matrix $\mathbf{D}^i$ is assumed to be linear. The assumption can be justified for a bone based on the linear load deformation curves obtained in the elastic region for a human femur subjected to uniaxial tension or compression and torsion loading tests [22].

## 3 The biomechanical model description

The three-dimensional lower body musculoskeletal model presented in this study is developed using the commercial software BRG.LifeMODE [17]. The software is based on the commercial multibody software ADAMS [23]. A graphic representation of the biomechanical model used in this study is shown in Fig. 1. The model is generated from the anthropometric database accessible through the software based on the experimental subject's height, weight, age, ethnicity, and gender. The model consists of seven segments as shown in Fig. 1. All of the segments are assumed to be rigid bodies except for the right tibia which is assumed to be a flexible body. The joints used to constrain the segments in the model in addition to their kinematic description are shown in Table 1. The joint resistance is modeled using a nonlinear torsional spring and torsional damper applied at each constraint degree of freedom in the model. The contribution of this torsional spring-damper is to guide the joint movement and keep it within its allowed physical angular limits [24]. The magnitude of the applied torsional spring varies with the joint orientation so that it is small at the initial joint orientation to permit joint deformation with minimal resistance, while it increases exponentially near the physical angular limits to protect the joint from exceeding impossible physical angles [24]. In the physical operating range of the joint, the torque varies linearly with the joint orientation [25]. The stiffness of the torques at the physical operating range of the joint can be defined experimentally based on the passive joint response. In this model, the stiffness of each joint within the allowable physical orientation is estimated based on the equations defined by Amankwah et al. [26], except for ankle inversion/eversion and hip rotation. For ankle inversion/eversion, a stiffness value of 10,000 Nmm/° is used to maintain the stability of the ankle joint in the inverse dynamics simulation, while the stiffness of the hip rotation is assumed to be 800 Nmm/°. This numerical value is obtained by studying the angular trajectory responses between the inverse and forward dynamics simulations. Table 2 shows the stiffness and damping values of the joints used. The present model is actuated by 12 muscle groups including 17 muscles. The muscle groups are: the soleus, gastrocnemius, tibialis anterior, biceps femoris, vastus lateralis, rectus femoris, iliacus, gluteus medius, gluteus maximus, adductor magnus, vastus medialis, and semitendinosus. The paths of the muscles (i.e., muscle origin and insertion sites) in addition to the muscles' physiological cross sectional areas are defined according to Eycleshymer and Schoemaker [27] and scaled to the model based on the anthropometric data of the experimental subject. The maximum muscle stress is assumed to be 87.1 N/cm$^2$ according to

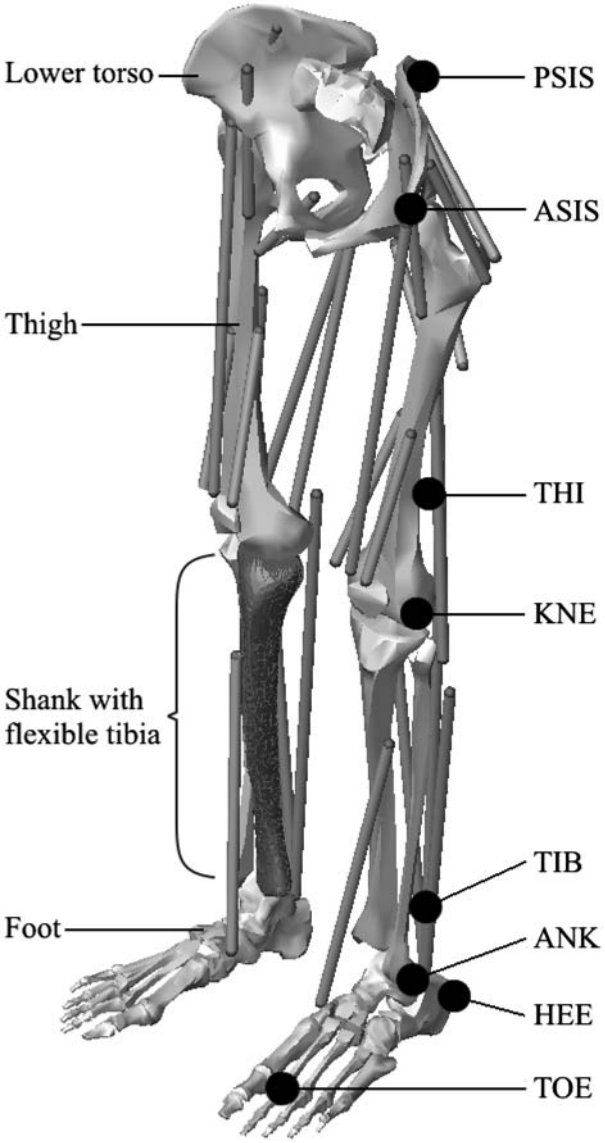


**Fig. 1** Graphic representation of the lower body musculoskeletal model used in this study with schematic illustration of motion capture marker placement. ASIS = anterior superior iliac spine, PSIS = posterior superior iliac spine, KNE = lateral epicondyle of the knee, THI = lower lateral 1/3 surface of the thigh, ANK = lateral malleolus, TIB = lower 1/3 of the shank, TOE = second metatarsal head, HEE = calcaneous at the same height as the toe marker

Hatze [28]. The foot-ground contact is modeled using five spring-damper systems located under each phalanx of the foot, in addition to one spring-damper system located under the heel of the foot. The stiffness, damping and full damping depth values are assumed to be 200 N/mm, 2 Ns/mm and 1 mm, respectively, and are based on the study of Gilchrist and Winter [29].

### 3.1 Flexible tibia

The geometrical configuration of the tibia is obtained from a three-dimensional reconstruction of MRI data taken from the sagittal plane from the right tibia of the subject. The MR

**Table 1** Kinematic constraints of the model

| Joint name | Type | Segments | | Motion | | |
|---|---|---|---|---|---|---|
| Hip | Spherical | Lower torso | Thigh | Flexion /extension | Abduction /adduction | Rotation |
| Knee | Revolute | Shank | Thigh | Flexion /extension | | |
| Ankle | Universal | Shank | Foot | Flexion /extension | Inversion /eversion | |

**Table 2** Joint stiffness and damping used for ankle, knee, and hip joints

| | Flexion/extension | | | Inversion/eversion Abduction/adduction | | | Rotation | | |
|---|---|---|---|---|---|---|---|---|---|
| | Stiffness (Nmm/°) | Damping (Nmms/°) | Neutral angle (°) | Stiffness (Nmm/°) | Damping (Nmms/°) | Neutral angle (°) | Stiffness (Nmm/°) | Damping (Nmms/°) | Neutral angle (°) |
| Ankle | 210 | 21 | 3.6 | 10,000 | 1,000 | NA | – | – | – |
| Knee | 270 | 27 | 7.2 | – | – | – | – | – | – |
| Hip | 700 | 70 | 5.0 | 1,500 | 150 | 7.8 | 800 | 80 | NA |

images are segmented using 3D-DOCTOR [30] to define the boundaries of the cortical tibial inner and outer surfaces. The boundary surfaces of the cortical tibia are processed to form a three-dimensional surface model of the tibia. The three-dimensional surface model consisting of the inner and outer cortical surfaces can be imported to SolidWorks [31] for smoothening to create a three-dimensional tibial solid model suitable for meshing. The three-dimensional tibial solid model can be imported to ANSYS [32] to describe the finite element model using a four-node tetrahedral solid element. Figure 2 shows the finite element model of the right tibia based on MRI data. In order to couple the flexible tibia to the adjacent bodies, massless nodes are modeled at the location of the ankle and knee joints. These nodes are selected as boundary nodal coordinates, and connected to the nodes at the surface of the tibial metaphyses using a number of massless rigid beams as shown in Fig. 2. These massless beams transform constraint forces due to the joints to the flexible tibia. A large number of massless rigid beams are used in order to ensure that the constraint forces due to the joints do not cause unnatural local deformation in the flexible tibia. The flexible tibia is used in the forward dynamics analysis to calculate deformation due to dynamic loading using (2.2). The material properties of the cortex bone are modeled to be linear elastic and transversely isotropic. Young's modulus and the shear elastic modulus of the cortex bone are assumed to be 17 GPa and 10 GPa, respectively, in the longitudinal direction along the bone, while they are assumed to be transversely isotropic with values of 5 and 3.5 GPa, respectively [33]. The total number of nodal degrees of freedom of the tibial finite element model is 16719 (i.e., $n = 16719$). The software (ANSYS) is used to calculate the number of Craig–Bampton modes employed in the floating frame of reference formulation. The strain energy method is used to select the significant deformation modes which describe the deformation of the tibia during the forward dynamics simulation [34]. A total number of 10 deformation modes (i.e., $m = 10$) are used in the numerical analysis. A critical damping ratio of 1 is applied to the selected modes based on the study of Dias Rodrigues et al. [35]. Figure 3 shows the selected tibial deformation modes with

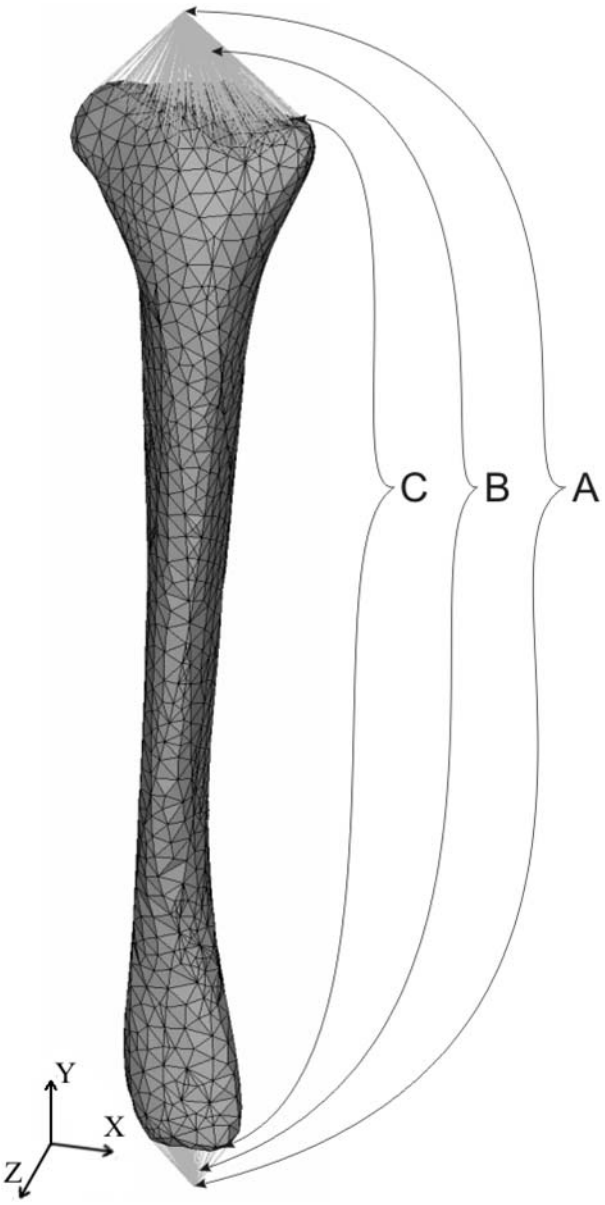


**Fig. 2** The tibial finite element model generated based on MRI and used in the forward dynamics simulation for strain analysis. A = two selected boundary nodes, B = massless rigid beams and C = surface nodes

their natural frequencies which are used in the forward dynamics analysis to obtain the tibial strains. In flexible multibody dynamics, the realistic geometry of the body plays a fundamental role in obtaining the correct deformation modes describing the flexibility of the body. Therefore, in this study, the tibial finite element model is developed using the actual geometry of the subject's tibia based on three-dimensional reconstruction of MRI data.

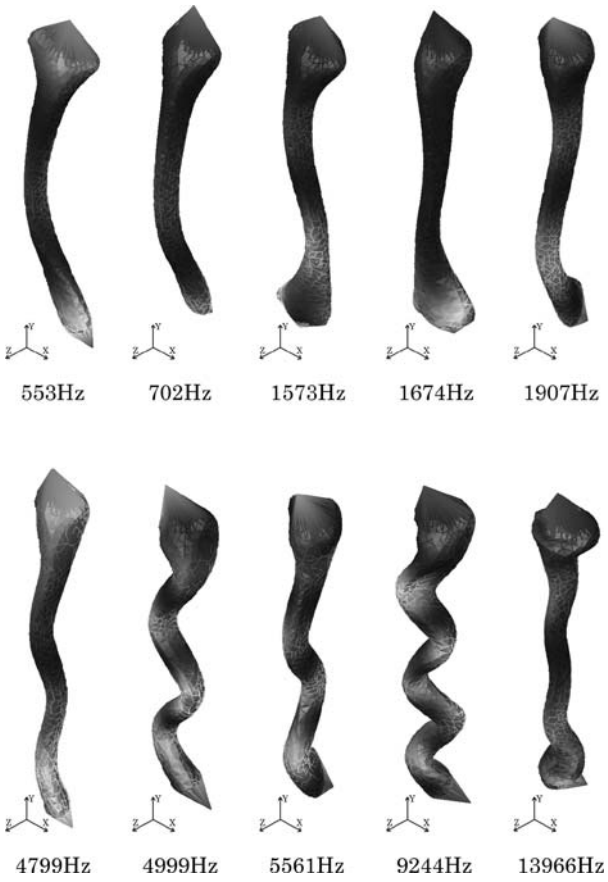


**Fig. 3** The selected tibial deformation modes with their natural frequencies

## 4 Numerical example

### 4.1 Human experiments

A healthy male volunteer (25 years, height 184 cm, mass 89 kg) was recruited for this study to perform level walking. The subject was asked to walk barefoot at a constant velocity (1.47 m/s) on a 10 m long force platform (Raute Inc., Finland) on level ground. The resultant ground reaction force and electromyographic (EMG) activity of the tibialis anterior, soleus, rectus femoris, vastus lateralis, biceps femoris, and gluteus medius muscles were recorded from the right side of the body. The gait was recorded with four digital video cameras (COHU High Performance CCD Camera, USA) at a 50 Hz sampling frequency. A schematic illustration of the measurement set up is provided in Fig. 4. Visual markers are applied on the lower body of the subject, as shown in Fig. 1. One walking cycle, from the heel strike of the right foot to the next heel strike, is selected for the analysis. The video clips from all four cameras are digitized using Peak Motus 8.1.0 (Peak Performance Technologies Inc., USA), and the software is used to calculate the three-dimensional coordinates for each marker. In order to minimize the digitization error, each of the coordinates is filtered with a second order 5 Hz low-pass Butterworth filter [36]. Successive walking cycles for one person can be assumed to have similar patterns [37]. Therefore, the coordinates are

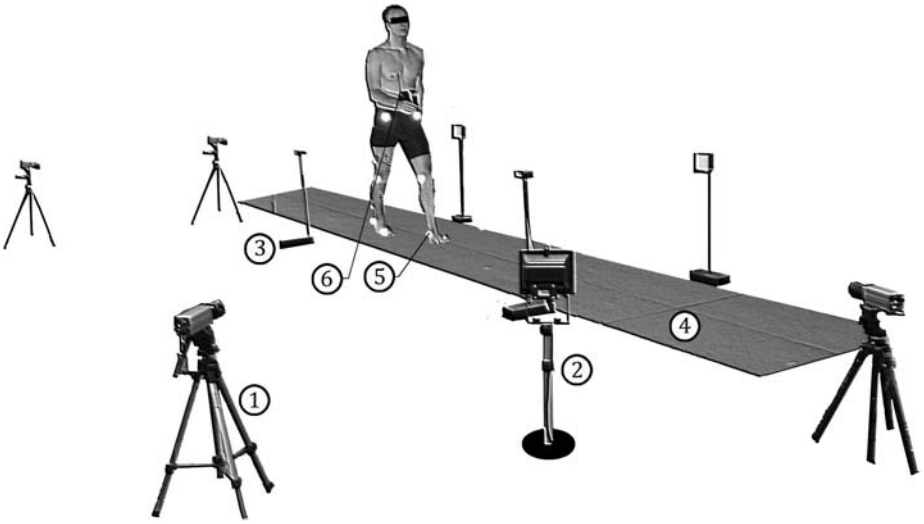


**Fig. 4** Schematic illustration of the experimental set up. *1*. Cameras. *2*. Light source. *3*. Photocells. *4*. Force platform. *5*. Visual markers. *6*. Telemetric EMG transmitter

interpolated so that coordinate data for a total of four identical walking cycles are produced. A total number of 250 sagittal MR images are taken from the right tibia of the subject with a slice thickness of 1.2 mm (Signa 1.5T Excite, GE Medical Systems, France) with intervals of 0.6 mm in the neutral unloaded position.

### 4.2 Simulation procedure

The simulation procedure employed to analyze the tibial strains during walking is described in the schematic diagram (Fig. 5). The simulation procedure comprises of both inverse and forward dynamics. The forward dynamics simulation is necessary for the purpose of this study in order to provide a realistic environment for the simulation in which the muscles are the prime actuators of the model. In the inverse dynamics analysis, the forces of different muscular groups can be lumped as moments about anatomical joints leading to a determinate inverse dynamics problem. The control method applied in the inverse dynamics simulation is the computed torque method [38]. The markers' trajectories serve as input for the inverse dynamics simulation. They are generated from three-dimensional motion capture data of markers placed at various locations on the subject (Fig. 1) and tracked during the walking test. From the joint moments (i.e., torques) and desired muscular contraction trajectories calculated in the inverse dynamics simulation the muscular forces can be obtained. The muscular forces are then used to drive the model in the forward dynamics simulation. To guarantee that the motion is reproduced in the forward dynamics simulation, the muscular forces are tracked using proportional derivative (PD) servo controller. The PD servo controller minimizes the error between the desired muscle contraction trajectory obtained from the inverse dynamics simulation and the instantaneous one obtained from the forward dynamics simulation at each simulation time step. In addition, it keeps each muscle force within its physiological limit (physiological cross sectional muscle area multiplied by maximum muscle stress). The lower body musculoskeletal model with a flexible tibia is employed in the forward dynamics simulation to predict the tibial strains resulting from level walking.

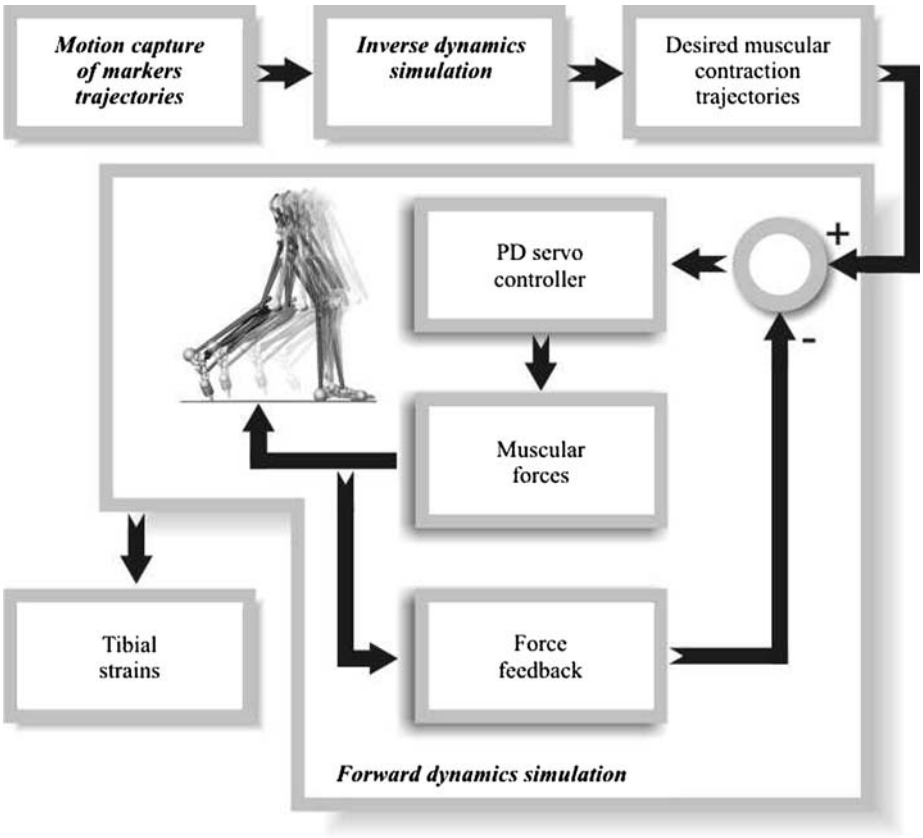


**Fig. 5** Schematic diagram of the simulation procedure used in this study

### 4.3 Numerical analysis

The principal strains are obtained from the model at a specified location, i.e., from the anteromedial aspect of the right tibial midshaft, corresponding to the location defined by Lanyon et al. [4], Burr et al. [5], and Milgrom et al. [39, 40]. The principal strains observed in the previous in vivo studies are calculated from the measured in plane strains using a rosette strain gauge bonded to the anteromedial aspect of the right tibial midshaft. Therefore, for the sake of comparison with the previous in vivo strain measurements, the principal and maximum shear strains are calculated based on the in plane strains obtained from the model using standard formulas [41]. To demonstrate the strain distributions around the cross section at the middle of the tibial shaft, the axial strain defined in the direction of the long axis of the tibia is simulated in four locations corresponding to the locations defined by Peterman et al. [42]. The muscular forces and the ground reaction force dominate the loading on the bone [43], which in turn determines the strain pattern. Therefore, in order to verify the accuracy of the introduced model, the ground reaction force and muscular activation patterns obtained from the model and experiment, respectively, are compared in terms of the cross-correlation coefficient ($\gamma$). Moreover, the model kinematics obtained from the inverse and forward dynamics simulations are compared in order to verify the model's capability of replicating the motion in forward dynamics simulation. This is accomplished by comparing

the center of mass location of each segment in the model in the $X$, $Y$, and $Z$ directions resulting from inverse dynamics simulation to their correspondences resulting from forward dynamics simulation in terms of $\gamma$.

## 5 Results and discussion

Four walking cycles are simulated using a simulation time step of 0.02 seconds. The values for the maximum and minimum principal strain, maximum shear strain and axial strain are obtained from the model. The numerical strain results obtained from the model and their correspondences reported from the previous in vivo strain measurements are given in Table 3. Figure 6 shows the simulated maximum and minimum principal and maximum shear strains for four walking cycles.

As regards the ground reaction force, the cross-correlation coefficient ($\gamma$) between measured and simulated values is 0.98. As for the muscular forces, a $\gamma$ of 0.88 is obtained for the soleus, 0.76 for the gluteus medius, 0.66 for the vastus lateralis, 0.38 for the tibialis, 0.33 for the biceps femoris, and 0.15 for the rectus. Simulated and measured muscular forces and ground reaction forces are plotted in Figs. 7 and 8. In the comparison of the model kinematics between inverse and forward dynamics simulations, the $\gamma$ is higher than 0.99 for the center of mass location of each segment in the model in the $X$, $Y$, and $Z$ directions.

### 5.1 Strain results

The study of Lanyon et al. [4] is apparently the first in vivo strain measurement on tibia for a normal subject during physical activities. In that study, walking on a belt without shoes at 1.4 m/s is one of the physical activities where tibial strains are assessed. The maximum principal and maximum shear strains obtained from the model differ by 23% and 14%, respectively, from the data reported by Lanyon et al. [4]. The profiles of the maximum and minimum principal strains seem to be similar to those reported by Lanyon et al. [4]. The oscillations in the strains produced by the model are apparently due to the fluctuations of the muscular forces. The study of Burr et al. [5] shows in vivo strain measurements in two subjects walking at 1.39 m/s and wearing heavy infantry boots weighing 1.2 kg. The difference between the values of the minimum principal strain and maximum shear strain obtained from

**Table 3** The principal strain magnitudes and rates. Literature values from in vivo measurements and the values estimated by the model in this study in addition to our previous study [16]. The principal strains and strain rates are obtained from the anteromedial aspect of the tibial midshaft, which is the same location in all of the studies mentioned in the table

| | Strain magnitude microstrain | | | Strain rate (microstrain/s) | | |
|---|---|---|---|---|---|---|
| | Max principal | Min principal | Max shear | Max | Min | Max shear |
| Lanyon et al. [4] | 395 | −434 | 829 | Not reported | −4,000 | Not reported |
| Burr et al. [5] | 437 | −544 | 871 | 11,006 | −7,183 | 16,162 |
| Milgrom et al. [39] | 840 | −454 | 1,183 | 3,955 | −3,306 | 10,303 |
| Milgrom et al. [40] | 394 | −672 | Not reported | 4,683 | −3,820 | Not reported |
| Al Nazer et al. [16] | 490 | −588 | 1,078 | 3,800 | −4,100 | 9,500 |
| Present simulation | 305 | −645 | 948 | 4,000 | −7,000 | 10,000 |

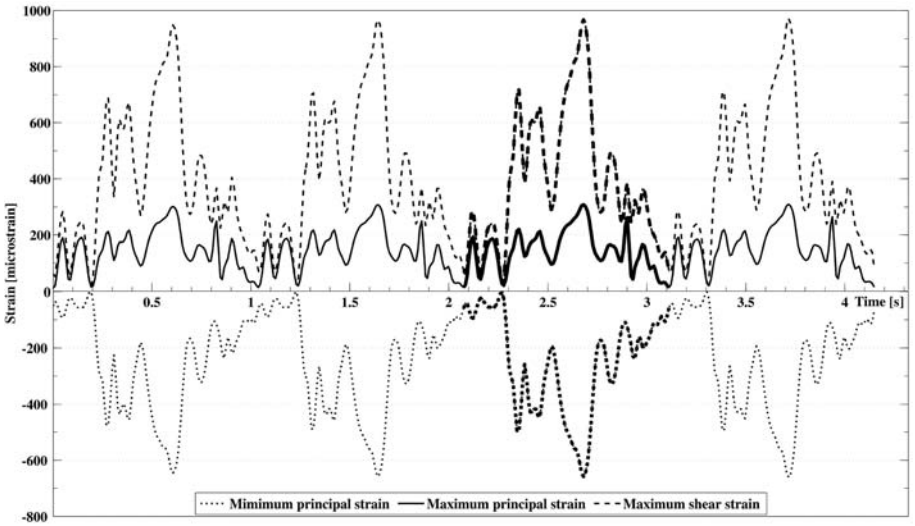


**Fig. 6** Simulated maximum, minimum principal strain and maximum shear strain curves at the anteromedial aspect of the right tibial shaft for four walking cycles. *Bolded line* corresponds for one walking cycle

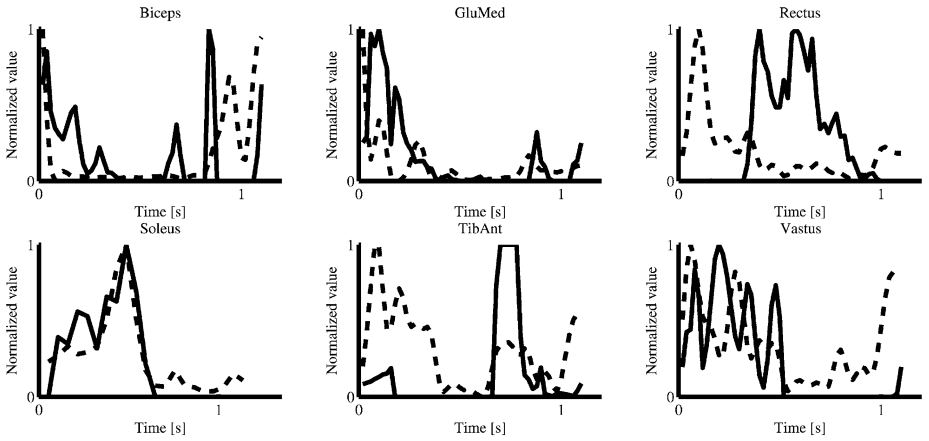


**Fig. 7** Measured electromyographical (EMG) muscle activity (*dashed line* - - -) and muscular force production obtained from the model (*solid line* —) plotted against time. EMG and force values were normalized to the maximum values for each plot. EMG is rectified and low pass filtered at 10 Hz. Biceps = biceps femoris, glumed = gluteus medius, rectus = rectus femoris, soleus = soleus, tibant = tibialis anterior and vastus = vastus lateralis

the model is 18% and 9%, respectively, compared to values presented by Burr et al. [5]. Yet the maximum shear strain curve obtained from the model appears to be comparable to the one obtained by Burr et al. [5]. It can be noticed that the strain rate magnitudes obtained by Burr et al. [5] are higher than their correspondences obtained from the model and the other in vivo strain measurement studies. However, the minimum strain rate obtained by the model differs only by 3% from the value reported by Burr et al. [5]. Milgrom et al. [39] present the tibial principal strains which are measured in vivo in six subjects walking with running

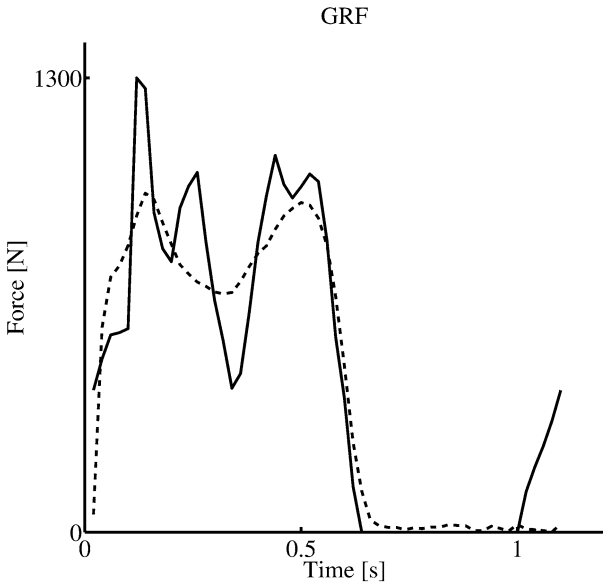


**Fig. 8** Measured ground reaction force (*dashed line* - - -) and simulated ground reaction force (*solid line* —) plotted against time for one walking cycle

shoes on a treadmill at 1.39 m/s. While the value of the maximum shear strain obtained from the model differs by 20% from its correspondence measured by Milgrom et al. [39], the maximum strain and maximum shear strain rates obtained from the model are within the range of ±2% of the values obtained by Milgrom et al. [39]. Furthermore, another recent study has been done in 2006 by Milgrom et al. [40] where the tibial principal strains and strain rates are measured in vivo for four male subjects walking with running shoes. The values of the maximum and minimum principal strains obtained from the model are different by 22% and 4% from corresponding data reported by Milgrom et al. [40], while the value of the maximum strain rate is 14% lower than the value reported from the same study. It is also noted that the estimated strain results reported in our previous study [16] are consistent with the strain results estimated from the present model. While the similarity could be expected, the estimated strain results from the present model may be considered more reliable as the actual geometrical configuration of the tibia is taken into account rather than the generic model used in our previous study [16]. Comparing the previous in vivo strain measurements during walking to the numerical results obtained from the present model, it can be concluded that the results obtained from the model are reasonable and consistent with the in vivo strain data. The differences between strain results may be explained by many factors, such as the subject's age, gender, height, and weight in addition to the experimental techniques used to measure the strains.

### 5.2 Strain distributions

In the study of Peterman et al. [42], the dynamic gait simulator described by Sharkey and Hamel [44] is used to measure the strain in vitro during the stance phase of walking from heel strike to toe off. In that study, five cadaver feet from different donors are harvested approximately 18 cm above the ankle and seven gage strain rosettes are bonded at the middle of each harvested tibial shaft (approximately 9 cm above the ankle) in seven locations around the cortex of the tibia. Axial strain profiles measured in the direction of the long axis of the tibia from four gages are reported in that study. Figure 9 shows the simulated axial

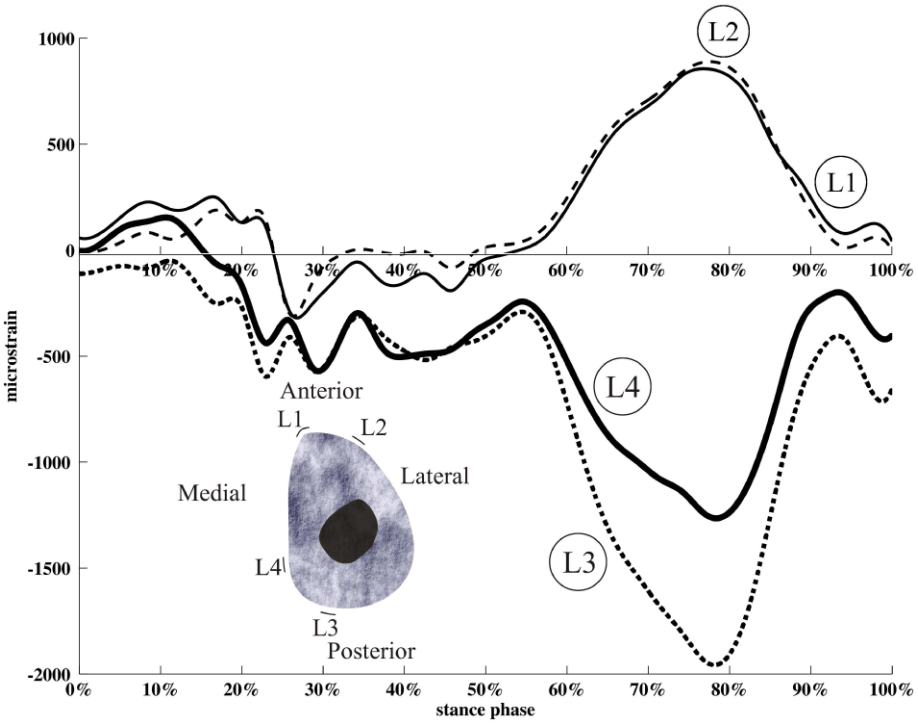


**Fig. 9** Simulated axial strain curves at the two anterior and two posterior sites around the cortical tibia at the middle of the tibial shaft during the stance phase. The shape represents the cortical cross sectional geometry at the middle of the subject's tibia

strain profiles at the middle of the tibia in four locations which correspond most closely to the locations defined by Peterman et al. [42]. The simulated strain profiles shown in Fig. 9 are similar to the profiles recorded in the study of Peterman et al. [42]. It is worth mentioning that strains at different distances between the ankle and the middle of the tibia are simulated using the presented model in the same locations around the cortical tibia defined by Peterman et al. [42] and their profiles were similar across all simulations and distance levels. Peterman et al. [42] state that they measured the strains around the cortical tibia at different distances 9, 12 and 15 cm above the ankle and their profiles were also similar across all measurements and mounting levels. Another concluding remark obtained from the model agreeing with what is stated in the study of Peterman et al. [42] is that the axial strains at the anterior location L1 has a similar profile to the maximum principal strain while axial strain at the posterior location L3 reflects the minimum principal strain. The strain distributions obtained from the introduced model indicate that bending is the primary mode of tibial loading, as it has been shown in other mammalian long bones according to the studies of Biewener [45] and Garcia and da Silva [46]. Based on the agreement between the predicted strains by the present model and the previous in vitro strain measurement study [42], it can be concluded that the model is able to predict the strain distributions around the cortical tibia under changing mechanical loading environment in the gait stance.

### 5.3 Validation of the biomechanical model

The accuracy of the biomechanical model is evaluated by comparing numerical results to measurements obtained from the practical experiment. The results have an acceptable overall agreement, whereas some discrepancy is observed between the measured muscular activities and modeled muscular force production patterns. The discrepancy between the tibialis anterior and biceps femoris forces obtained from the model and their EMG measured from the experiment may be caused by the algorithm used to solve the muscular force production. The algorithm is based on changes in muscle length and for this reason did not account for the coactivation of muscles. The discrepancy found in the rectus femoris may be attributed to the fact that only the lower body musculoskeletal model is used, and the psoas major muscle is not included in the muscle set used in the model. Consequently, the rectus femoris muscle had to take the role of the psoas major muscle in providing the necessary moment for hip flexion leading to overreaction noticed in the rectus femoris pattern.

### 5.4 Limitations of the biomechanical model

The accuracy of this approach is mainly limited by the estimation procedure of muscular forces. This is due to the fact that extensive description of a human musculoskeletal model including the skeleton and many muscle groups for the simulation of human motions still remains an ambitious and challenging task. Moreover, this approach employs motion capture of the subject's body kinematics. This task may not be possible in some environments due to the high costs of the measurement systems, or due to technical difficulties such as external activities. Another general limitation can arise from the fact that the proposed approach in this study requires employing the forward dynamics simulation for bone strain analysis. This is because the forward dynamics simulation provides a realistic environment in which the muscles are the prime actuators of the model. In some cases where the biomechanical model involves more complex muscle model, the forward dynamics simulation might become expensive, especially in the cases where dynamic optimization techniques are used [24, 47]. Nevertheless, the strain magnitudes obtained by the present approach are consistent with corresponding data obtained from the previous in vivo measurements [4, 5, 39, 40].

## 6 Conclusions

The bone strain environment plays a crucial role in the process of bone remodeling and modeling. While the in vivo tibial strain measurement is an invasive procedure and requires surgical implementation of strain gauges and involves risks (e.g., infection), the present flexible multibody approach appeared to perform reasonably in estimating dynamic bone strains. The integration of the MR imaging technique improves the accuracy of the finite element model of the bone and simulation of bone strains, as the flexible bone model reflects the realistic geometry of the bone. There are a number of future opportunities for research and development with the potential for developing other flexible multibody biomechanical models employing the MR imaging technique. These could include the following medical applications: (1) assessing the strain patterns in bones that are not directly accessible in vivo; (2) designing targeted physical training exercises (i.e., those producing a desired strain pattern) to improve skeletal rigidity; (3) developing implants by applying dynamic strain analysis to assess how the implant material behaves under loading, and (4) performing detailed internal strain analysis, e.g., in the field of joint prostheses. A detailed strain analysis

might require quantitative computed tomography (QCT) scanning of the bone so that the inhomogeneous density and elasticity distribution of the bone as well as its internal structure could be better considered. Finally, we hypothesize that a more sophisticated muscle model and attachments as well as bone material properties could further lead to a more accurate simulation of bone strains using the flexible multibody approach presented in this study.

## Conflict of interest statement

All authors have no conflict of interests.

**Acknowledgements** The project was funded by the Academy of Finland (# 114925). The authors would like to thank Dr. Matti Sauna-Aho for his assistance and help.

## References

1. Leondes, C.: Musculoskeletal Models and Techniques. Biomechanical Systems: Techniques and Applications, vol. III. CRC Press, Boca Raton (2000)
2. Turner, C.H.: Three rules for bone adaptation to mechanical stimuli. Bone **23**, 399–407 (1998)
3. Lanyon, L.E., Rubin, C.T.: Static vs dynamic loads as an influence on bone remodeling. J. Biomech. **17**, 897–905 (1984)
4. Lanyon, L.E., Hampson, W.G., Goodship, A.E., Shah, J.S.: Bone deformation recorded in vivo from strain gauges attached to the human tibial shaft. Acta Orthop. Scand. **46**, 256–268 (1975)
5. Burr, D.B., Milgrom, C., Fyhrie, D., Forwood, M., Nyska, M., Finestone, A., Hoshaw, S., Saiag, E., Simkin, A.: In vivo measurement of human tibial strains during vigorous activity. Bone **18**, 405–410 (1996)
6. Földhazy, Z., Arndt, A., Milgrom, C., Finestone, A., Ekenman, I.: Exercise-induced strain and strain rate in the distal radius. J. Bone Jt. Surg. **87-B**, 261–266 (2005)
7. Eberhard, P., Spägele, T., Gollhofer, A.: Investigations for the dynamical analysis of human motion. Multibody Syst. Dyn. **3**, 1–20 (1999)
8. Piazza, S.J., Delp, S.L.: Three-dimensional dynamic simulation of total knee replacement motion during step-up task. J. Biomech. Eng. **123**, 599–606 (2001)
9. Delp, S.L.: Surgery simulation: A computer graphics system to analyze and design musculoskeletal reconstructions of the lower limb. Doctoral thesis, Stanford University (1990)
10. Spagele, T., Kistner, A., Gollhofer, A.: Modeling, simulation and optimisation of a human vertical jump. J. Biomech. **32**, 521–530 (1999)
11. Nagano, A., Yoshioka, S., Komura, T., Himeno, R., Fukashiro, S.: A three-dimensional linked segmental model of the whole human body. Int. J. Sport Health Sci. **3**, 311–325 (2005)
12. Silva, M.P.T., Ambrósio, J.A.C., Pererira, M.S.: Biomechanical model with joint resistance for impact simulation. Multibody Syst. Dyn. **1**, 65–84 (1997)
13. Ambrósio, J.A.C., Silva, M.P.T.: Structural and biomechanical crashworthiness using multi-body dynamics. Proc. Inst. Mech. Eng. Part D J. Automob. Eng. **218**, 629–645 (2004)
14. Duda, G.N., Heller, M., Albinger, J., Schulz, O., Schneider, E., Claes, L.: Influence of muscle forces on femoral strain distribution. J. Biomech. **31**, 841–846 (1998)
15. Cheung, J.T., Zhang, M., Leung, A.K., Fan, Y.B.: Three-dimensional finite element analysis of the foot during standing—a material sensitivity study. J. Biomech. **38**, 1045–1054 (2005)
16. Al Nazer, R., Rantalainen, T., Heinonen, A., Sievänen, H., Mikkola, A.: Flexible multibody simulation approach in the analysis of tibial strain during walking. J. Biomech. **41**, 1036–1043 (2008)
17. LifeMOD User's Manual, version 2007.0.0, Biomechanics Research Group, Inc., California, USA (2007)
18. Shabana, A.A.: Dynamics of Multibody Systems. Cambridge University Press, New York (1998)
19. De Jalon, J.G., Bayo, E.: Kinematic and Dynamic Simulation of Multibody Systems: The Real Time Challenge. Springer, New York (1994)
20. Kim, S., Haug, E.J.: Selection of deformation modes for flexible multibody dynamics. Mech. Struct. Mach. **18**, 565–586 (1990)
21. Craig, R.R.: Coupling of substructures for dynamic analysis—an overview. American Institute of Aeronautics and Astronautics Dynamics Specialists Conference, Atlanta, USA (2000)

22. Reilly, D.T., Burstein, A.H.: The elastic and ultimate properties of compact bone tissue. J. Biomech. **8**, 393–405 (1975)
23. ADAMS Online Documentation, version 12.0, Mechanical Dynamics, Inc., Ann Arbor, Michigan, USA (2001)
24. Pandy, M.G.: Computer modeling and simulation of human movement. Annu. Rev. Biomed. Eng. **3**, 245–273 (2001)
25. Nigg, B.M., Herzog, W.: Biomechanics of the Musculo-Skeletal System. Wiley, New York (1999)
26. Amankwah, K., Triolo, R.J., Kirsch, R.: Effects of spinal cord injury on lower-limb passive joint moments revealed through a nonlinear viscoelastic model. J. Rehabil. Res. Dev. **41**, 15–32 (2004)
27. Eycleshymer, A.C., Shoemaker, D.M.: A Cross-section Anatomy. Appleton-Century-Crofts, New York (1970)
28. Hatze, H.: Estimation of myodynamics parameter values from observations on isometrically contracting muscle groups. Eur. J. Appl. Physiol. Occup. Physiol. **46**, 325–338 (1981)
29. Gilchrist, L.A., Winter, D.A.: A two-part, viscoelastic foot model for use in gait simulations. J. Biomech. **29**, 795–798 (1996)
30. 3D-DOCTOR User's Manual, version 4.0, Able Software Corp., Lexington, USA (2007)
31. SolidWorks User's Manual, version SP3.1, Dassault Systemes, Sureness, France (2005)
32. ANSYS User's Manual, version 11.0, ANSYS Inc., Canonsburg, USA (2001)
33. Dong, X.N., Guo, X.E.: The dependence of transversely isotropic elasticity of human femoral cortical bone on porosity. J. Biomech. **37**, 1281–1287 (2004)
34. Meirovitch, L.: Elements of Vibration Analysis. McGraw-Hill, New York (1975)
35. Dias Rodrigues, J.F., Lopes, H., De Melo, F.Q., Simoes, J.A.: Experimental modal analysis of a synthetic composite femur. Soc. Exp. Mech. **44**, 29–32 (2004)
36. Silva, M.P.T., Ambrósio, J.A.C.: Kinematic data consistency in the inverse dynamics analysis of biomechanical systems. Multibody Syst. Dyn. **8**, 219–239 (2002)
37. Vaughan, C.L., Davis, B.L., O'Connor, J.C.: Dynamics of Human Gait. Kiboho, Cape Town (1999)
38. Wasfy, T.M., Noor, A.K.: Computational strategies for flexible multibody systems. Appl. Mech. Rev. **56**, 553–613 (2003)
39. Milgrom, C., Finestone, A., Simkin, A., Ekenman, I., Mendelson, S., Millgram, M., Nyska, M., Larsson, E., Burr, D.: In-vivo strain measurements to evaluate the strengthening potential of exercises on the tibial bone. J. Bone Jt. Surg. **82**, 591–594 (2000)
40. Milgrom, C., Radeva-Petrova, D.R., Finestone, A., Nyska, M., Mendelson, S., Benjuya, N., Simkin, A., Burr, D.: The effect of muscle fatigue on in vivo tibial strains. J. Biomech. **40**, 845–850 (2006)
41. Hibbeler, R.C.: Mechanics of Materials. Prentice-Hall, Singapore (2005)
42. Peterman, M.M., Hamel, A.J., Cavanagh, P.R., Piazza, S.J., Sharkey, N.A.: In vitro modeling of human tibial strains during exercise in micro-gravity. J. Biomech. **34**, 693–698 (2001)
43. Burr, D.B.: Muscle strength, bone mass, and age-related bone loss. J. Bone Miner. Res. **12**, 1547–1551 (1997). Official Journal of the American Society for Bone and Mineral Research
44. Sharkey, N.A., Hamel, A.J.: A dynamic cadaver model of the stance phase of gait: performance characteristics and kinetic validation. Clin. Biomech. **13**, 420–433 (1998)
45. Biewener, A.A.: Musculoskeletal design in relation to body size. J. Biomech. **24**, 19–29 (1991)
46. Garcia, G.J., da Silva, J.K.: On the scaling of mammalian long bones. J. Exp. Biol. **207**, 1577–1584 (2004)
47. Ackermann, M.: Dynamics and energetics of walking with prostheses. Doctoral Thesis, University of Stuttgart (2007)